J Solid State Electrochem (2012) 16:1219–1228
DOI 10.1007/s10008-011-1516-3

ORIGINAL PAPER

Fabrication parameter-dependent morphologies of self-organized ZrO_2 nanotubes during anodization

Dong Fang · Jingang Yu · Zhiping Luo · Suqin Liu · Kelong Huang · Weilin Xu

Received: 1 December 2010 / Revised: 25 July 2011 / Accepted: 27 July 2011 / Published online: 9 August 2011

Abstract Zirconia (ZrO_2) nanotubes have been synthesized using a facile anodizing process in organic electrolyte systems containing a low content of fluoride. The nanotube architecture evolution was recorded at different anodization periods (1–24 h) by scanning electron microscopy. A compact layer was found between the Zr substrate and its upper tubular layer after 1 h of anodization, whereas after further anodization for 3 h the compact layer disappeared. Meanwhile, ZrO_2 nanotubes turned to a uniform structure from top to bottom. However, after 18–24-h-long anodization, the uniform tubular layer was replaced by a random layer composed of various structural defects. Since the compact layer was not completely dissolved, the retained compact layer yielded O-rings with double walls on the outer surface of the nanotubes.

Keywords Anodization · Electron microscopy · Fabrication parameter · Mechanism · Morphology · ZrO_2 nanotube

Introduction

Anodization is a common method to fabricate porous oxide nanostructures on the surface of valve metals, including aluminum [1], titanium [2], tantalum [3], niobium [4], zirconium [5], tungsten [6], and hafnium [7, 8], etc. Anodic zirconia (ZrO_2) nanotubes have high surface areas which may improve their properties in certain applications [9, 10], such as gas sensors [11], fuel cells [12], thermal barrier coatings [13], refractory materials [14], and catalysts [15]. As a result, great efforts have been made to prepare ZrO_2 nanotubes by anodization in fluoride or chlorine ion-containing electrolytes [5, 16–20]. The past endeavours focused on the ZrO_2 microstructure and morphology (size and length of nanotubes) by adjusting the anodization conditions such as electrolytic composition [21], applied potential [17], sweep rate [5, 22], and anodization time [23], while details about the growth mechanisms and film composition remain unclear [24].

In this study, ZrO_2 nanotubes were fabricated by anodization of Zr substrate. The nanotube architecture evolution during the anodization process was presented and the formation mechanism was explicated. The ZrO_2 nanotubes were characterized using scanning electron microscopy (SEM), X-ray diffraction (XRD), X-ray energy dispersive spectrometer (EDX), and transmission electron microscopy (TEM).

Experimental

Preparation of ZrO_2 nanotubes

Zr foils (99.6% purity, 0.3 mm in thickness) were degreased by sonication in acetone, isopropanol, and methanol. This procedure was followed by rinsing with deoinized water (D.I. water) and drying in air. The electrochemical setup consisted of a two-electrode configuration with graphite gauze as a counter-electrode. Two electrolytes were used in our experiments: (1) a mixture of glycerol and formamide

D. Fang · W. Xu
Key Lab of Green Processing and Functional Textiles of New Textile Materials, Ministry of Education,
Wuhan Textile University,
430073, Wuhan, China

D. Fang · J. Yu · S. Liu (✉) · K. Huang
College of Chemistry and Chemical Engineering,
Central South University,
Changsha 410083, People's Republic of China
e-mail: csufangdong@gmail.com

Z. Luo
Microscopy and Imaging Center and Materials Science and Engineering Program, Texas A&M University,
College Station, TX 77843, USA

(weight ratio=1:1) containing 1 wt.% NH_4F and 3 wt.% H_2O and (2) a mixture of glycol and formamide (weight ratio=4:1) containing 1 wt.% NH_4F and 1 wt.% H_2O. The anodization temperature and other parameters were specified in each experiment. During the anodization process, the solution was rigorously mixed using a magnetic stirrer. Upon the completion of the anodization, the samples were taken out from the electrolyte, rinsed with anhydrous ethanol for three times, and dried in air. Afterwards, the samples were sonicated in anhydrous ethanol for 10 min, taken out from the solution, and then dried in air.

Characterization

Scanning electron microscopy (Quanta 600, FEI) with an X-ray energy dispersive spectrometer (INCA program from Oxford Instruments) was used to examine the morphology and composition of the samples. A thin Au layer (3 nm) was coated on the specimens to increase conductivity by a sputter coater (K575X, Emitech, UK). During EDX characterization, the accelerated voltage was 15–20 kV and the working distance was 10 mm. The detected energies ranged from 0 to 20 keV and the dwell time was 3 min. Transmission electron microscope (JEM-2100, JOEL) was also used to examine the morphology of the samples. For TEM characterization, the samples were separated by ultrasonically dispersing in D.I. water, and then a drop of the solution was placed on a Cu grid covered with carbon film. X-ray diffraction measurement was carried out on a MXPAHF X-ray diffractometer with CuKα radiation (λ=1.54056 Å). The chemical composition of the samples was also analyzed by X-ray photoelectron spectroscopy (XPS, K-Alpha 1063, Thermo Fisher Scientific, UK).

Results and discussion

Figure 1a–c shows representative SEM images of the as-prepared ZrO_2 nanotube arrays formed at 50 V in a mixture

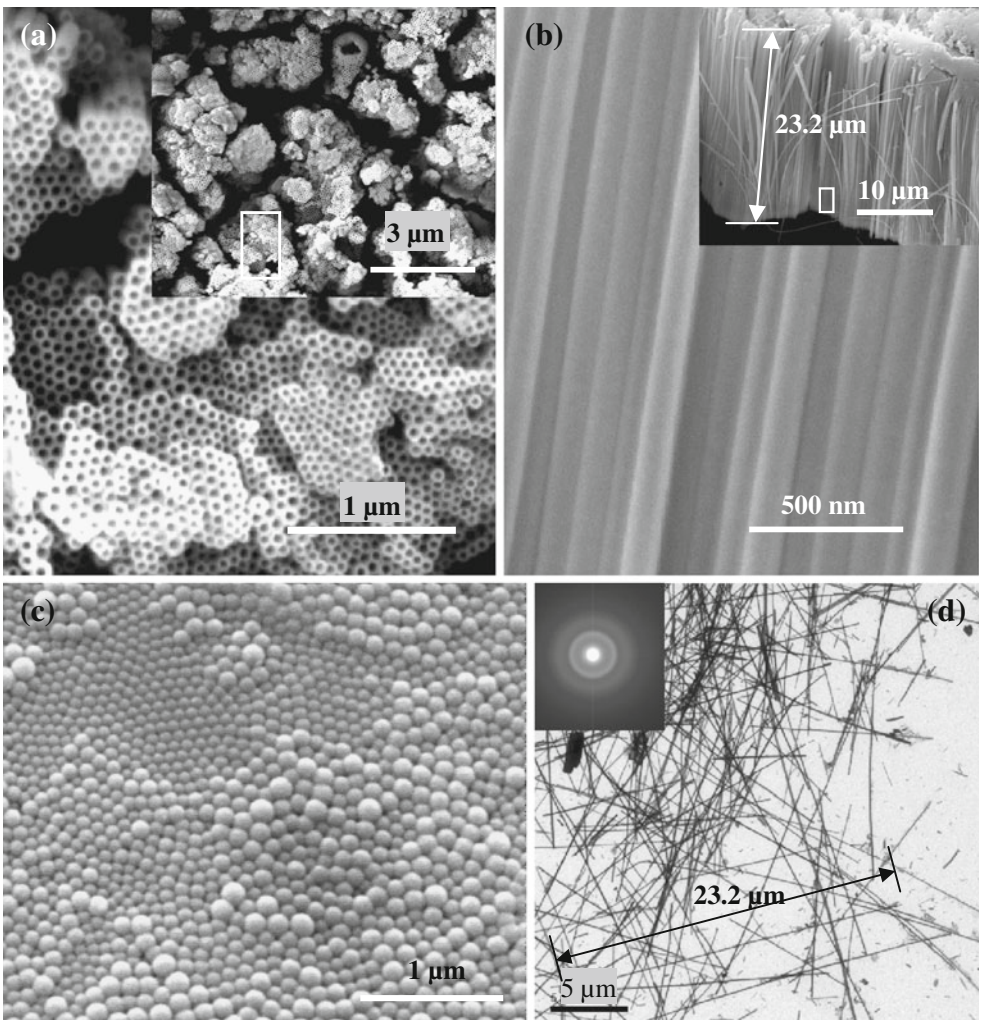

Fig. 1 SEM images of the as-prepared ZrO_2 nanotubes grown by anodization for 3 h in a mixture of glycerol and formamide (weight ratio=1:1) at room temperature, along the top view (**a**), cross-sectional view (**b**), and bottom view (**c**). A TEM image of the as-prepared ZrO_2 nanotubes is shown in **d**, with an SAED pattern inserted. The *inset* in **b** shows the thickness of the nanotubes

of glycerol and formamide (weight ratio=1:1) containing 1 wt. % NH_4F and 3 wt.% H_2O. The top surface of the ZrO_2 nanotube arrays is shown in Fig. 1a, where it can be seen that the arrays consisted of regular tubes. The length of the ZrO_2 nanotubes is about 23.2 μm, as shown in the inset of Fig. 1b. The backside of the ZrO_2 nanotubes is shown in Fig. 1c. It is seen that the bottoms of the nanotubes are closed. Figure 1d is a TEM image of the ZrO_2 nanotubes. From the selected-area electron diffraction (SAED) pattern inserted in Fig. 1d, the nanotubes are recognized as amorphous.

To explore the feasibility to tailor the morphology, especially to investigate the relationship between the nanotube length and the anodizing time, we repeated the nanotube layer growth process six times using a potential sequence. Each anodizing process was conducted at 50 V for 10 min after switching on the circuit for 1 min (Fig. 2a). Figure 2b shows the SEM image of the obtained structure. Clearly, a multilayer morphology consisting of four and half layers is observed. As we repeated the experiment six times, six layers are expected. Therefore, the first one and half layers might be dissolved during the initial stage of the experiment. The length of the third to the sixth layer was about 6.4, 6.1, 5.0, and 4.2 μm, respectively. The speed of fabricating ZrO_2 nanotubes decreased with a longer anodic oxidation time. The length of the first and second layer were expected to be longer than 6.4 μm (the length of the third layer), while only 3.2 μm remains as shown in Fig. 2c, and thus we could estimate that the dissolving speed at the membrane surface was more than 9.6 μm within the first hour $(6.4 \times 2 - 3.2 = 9.6\ \mu m)$. At the same time, the nanotubes near the third/fourth layer junction were not smooth, with the presence of small particles on their walls (Fig. 2c). However, the nanotubes near the fifth/sixth layer junction are smooth (Fig. 2d). This morphology difference should be further studied.

The cross-sectional SEM images when the anodizing time is extended to 18 and 24 h to compare the morphologies of the ZrO_2 nanotubes during anodizations are shown in Fig. 3. The cross-sectional view in Fig. 3a indicates that the sample fabricated at 50 V for 18 h has two layers. The top layer is a uniform tubular layer, as magnified in Fig. 3b, and the bottom layer is a random layer with many particles, as magnified in Fig. 3c. However, when the sample is fabricated at 50 V for 24 h, the top uniform tubular layer even disappears (Fig. 3d–f). The color of the membranes on the Zr substrates fabricated for 18 and 24 h turns to white, which is in contrast to the yellow membranes fabricated for 3 h.

In order to clarify the morphology architecture transformation of ZrO_2 nanotubes during anodization, ZrO_2 nanotubes were fabricated at 50 V for 1 h in a mixture of glycerol and formamide (weight radio=1:1), and then the samples were transferred into anhydrous ethanol to wash

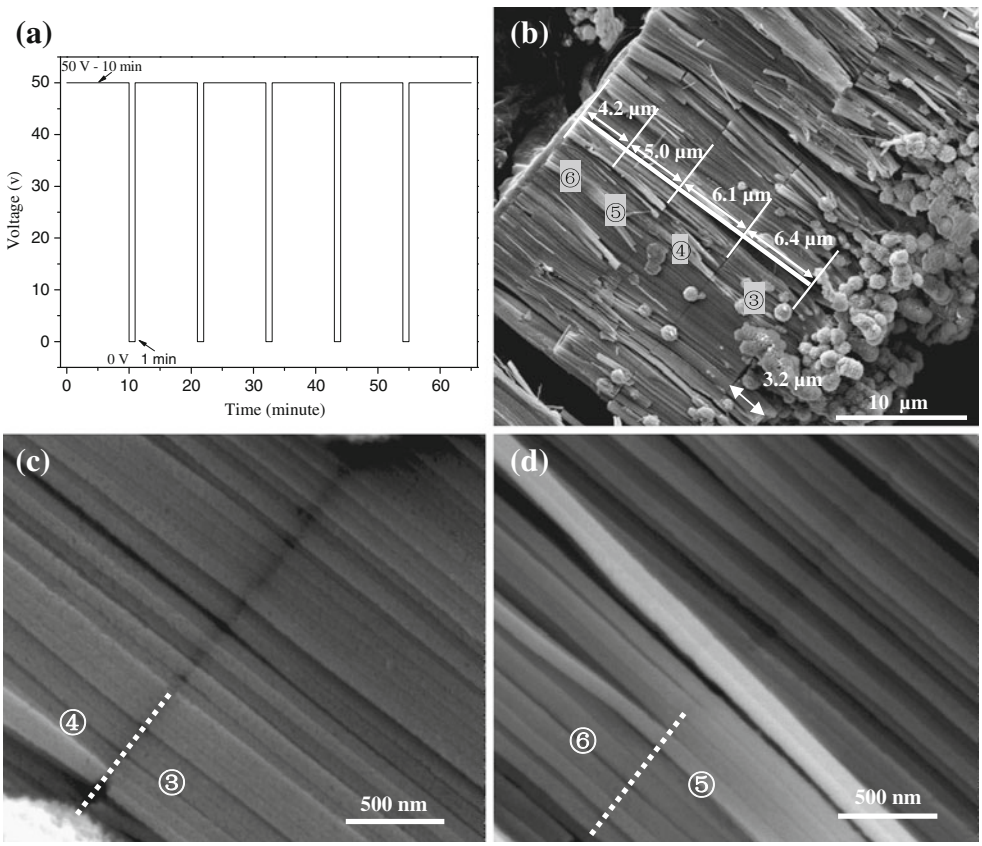

Fig. 2 **a** Each anodization process was conducted at 50 V for 10 min after opening the circuit for 1 min. **b** Cross-sectional SEM images of the ZrO_2 multilayers prepared by the combination of six anodization processes for Zr in a mixture of glycerol and formamide (weight ratio=1:1). The cross-sectional SEM images of the ZrO_2 nanotubes near the third/fourth layer junction (**c**) and the nanotubes near the fifth/sixth layer junction (**d**)

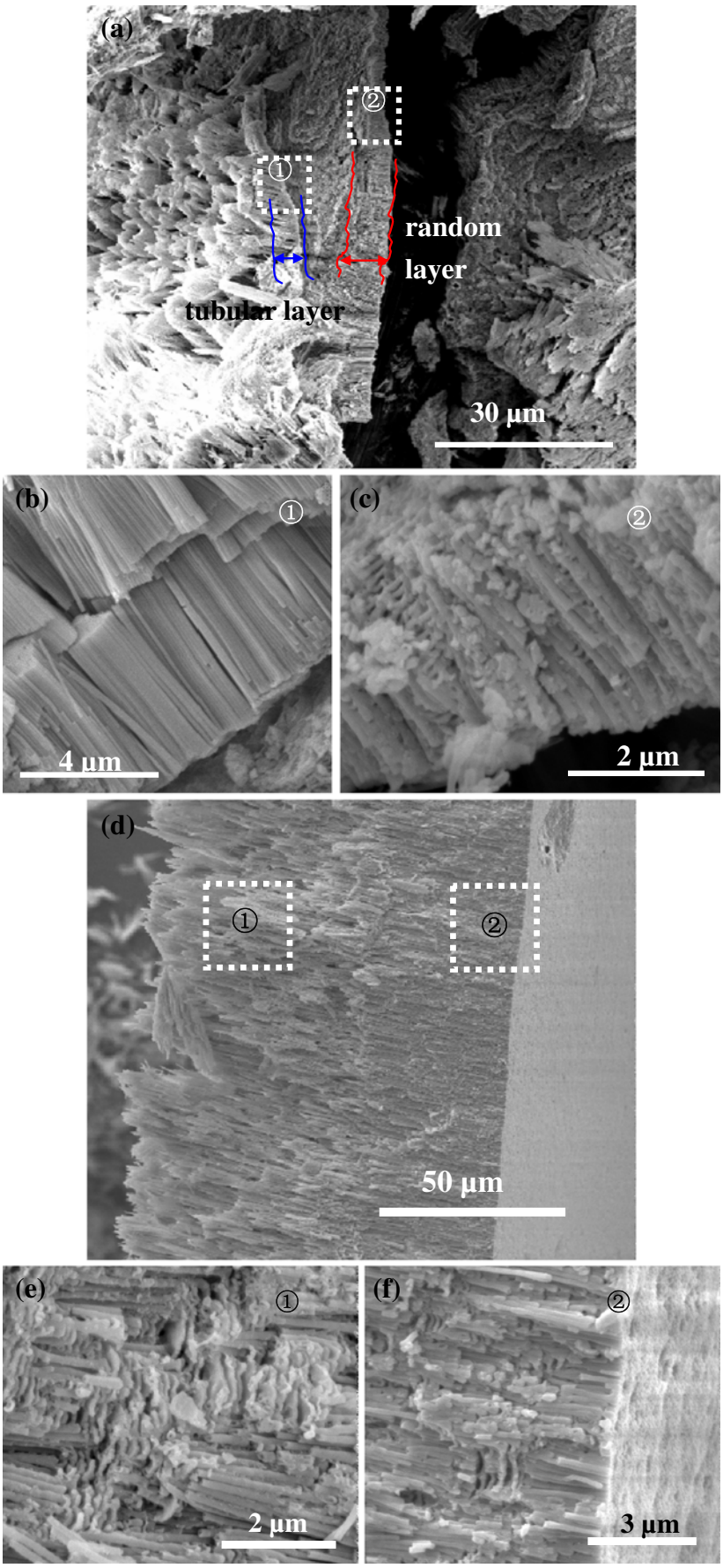

Fig. 3 Cross-sectional SEM images of ZrO_2 nanotubes prepared by anodization processes under 50 V for 18 h (**a**, **b**, **c**) and 24 h (**d**, **e**, **f**) in a mixture of glycerol and formamide (weight ratio=1:1) at room temperature

off the electrolyte. After the samples were washed with anhydrous ethanol, the cross-sectional and bottom SEM images of ZrO_2 nanotubes are shown in Fig. 4a, b, respectively. A compact layer is found under the tubular layer, with thickness of about 100 nm, as shown in the cross-sectional view in Fig. 4a. At the bottom as shown in Fig. 4b, part of the compact layer is detached from the nanotube bottoms during preparation of the SEM sample. EDX analysis was used to identify the elements of the compact layer. The EDX spectrum from the tubular layer depicts a higher O peak but a lower F peak, as shown in Fig. 4c, while the compact layer depicts a lower O peak but a higher F peak. Their Zr peaks remain of the same intensity. Therefore, the compact layer has relatively higher fluorine than that in the tubular layer. The fluorine may come from stable zirconium oxyfluorides or even zirconium fluorides. Subsequently, the ZrO_2 nanotube membrane was detached from the Zr substrate using an adhesion tape and the XRD spectrum of the membrane is presented in Fig. 4e. From the XRD result, the membrane has an amorphous structure without any evidence of Zr metal, indicating that the compact layer does not have any residual Zr metal attached to the nanotube bottom.

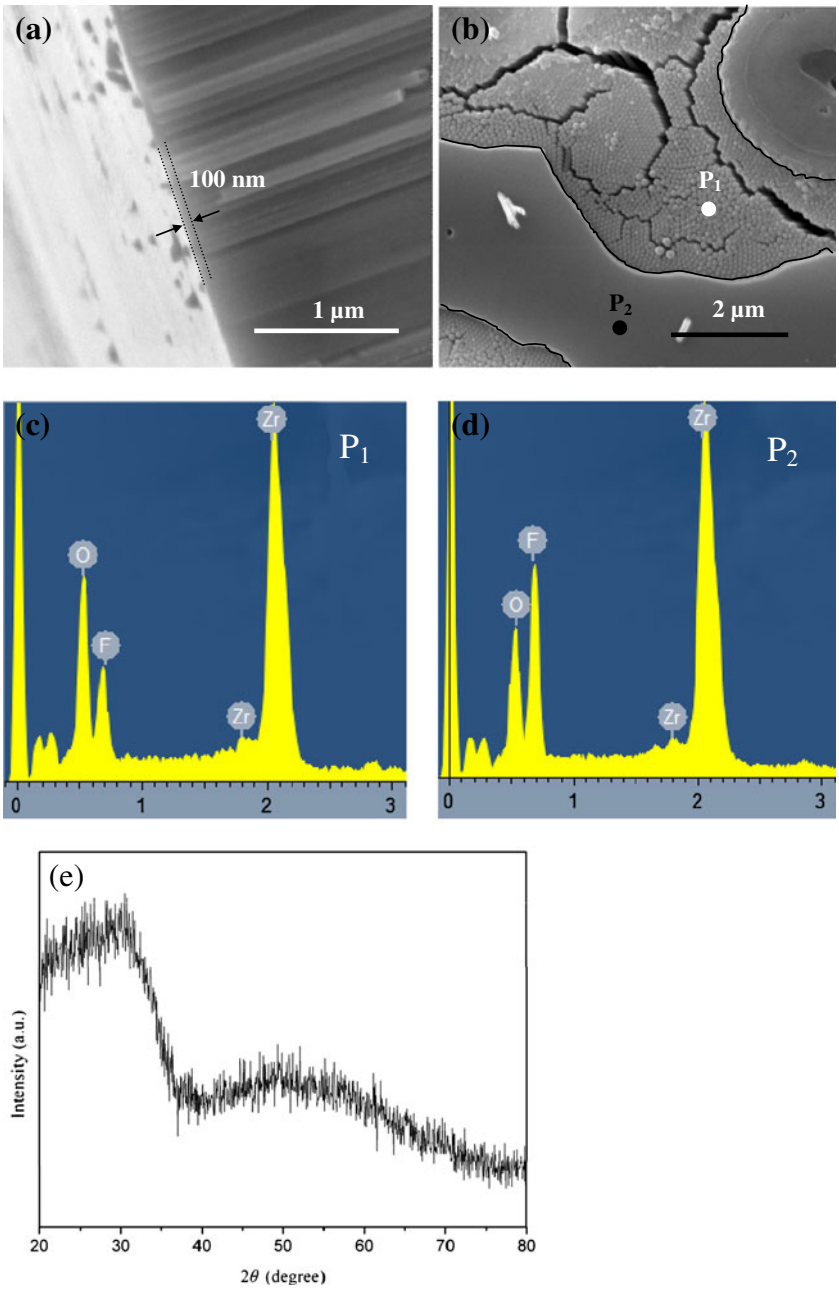

Fig. 4 SEM images of cross-sectional view (**a**), bottom view (**b**), EDX spectra (**c**, **d**), and XRD pattern (**e**) of ZrO_2 nanotubes fabricated at 50 V for 1 h in a mixture of formamide and glycerol (weight ratio=1:1) at room temperature

The anodic ZrO_2 nanotubes are also fabricated in a mixture of glycerol and formamide (weight ratio=1:1) at 0 °C and 30 for 1 h. The nanotubes fabricated at 0 °C exhibit a rough surface with some small particles on their walls, with a thin compact layer (about 310 nm) under the tubular layer, as shown in Fig. 5a, b, whereas the nanotubes fabricated at 30 °C have a smooth surface, as shown in Fig. 5c, d, with a thicker compact layer (910 nm) under the tubular layer similar to the sample prepared at 20 °C. The outer diameter of the nanotubes fabricated at 30 °C is about 130 nm, which was larger than that fabricated at 0 °C of about 105 nm.

To examine the anodizing potential effect, 20 and 60 V were applied as operating voltages in the experiment. It was found that the anodic ZrO_2 film fabricated at 20 V, as shown in Fig. 6a, b, does not have a compact layer under the tubular layer, while a compact layer is present on the bottom of the film fabricated at 60 V, as shown in Fig. 6c, d. It was reported that, in an anodizing process, the applied voltage plays an important role in determining the dimensions and shape of the pore [25]. If the electric field across the layer was strengthened, the rate of migration of cations and/or anions would speed up accordingly. During the growth of zirconia, Zr^{4+} movement is negligible whereas the growth occurs mostly at the metal/oxide interface via the inwards transport of F^- and O^{2-} across the growing layer [26, 27]. Upon reaching the opposite side of the oxide, F^- and O^{2-} react with cations, forming additional fluoride and oxide phases at the oxide/metal interface. Furthermore, a compact layer is formed between the Zr substrate and the tubular layer [28].

Based on the experimental observations, we suggest a model to elucidate the morphological architecture evolution of ZrO_2 nanotubes on a Zr substrate during anodization, which is schematically presented in Fig. 7. After 1 h of anodization, a fluorine-rich layer is found under the tubular layer. After 3 h more of anodization, the fluorine-rich layer disappears and an entire uniform tubular layer on a Zr substrate is formed, while after 18 h of anodization a random layer with various defects appears under the top tubular layer on a Zr substrate, and after 24 h more of anodization the top tubular layer disappears, which is replaced with an entirely random layer composed of structural defects. There are three anions (O^{2-}, OH^-, and F^-) in the electrolyte whose migration depends on the discharge of ions at the oxide/electrolyte interface, as well as their charge, size, and content in the electrolyte [29]. Shimizu et al. [30] found that fluoride ions moved inward with an average mobility 1.85 times faster than that of oxygen ions in growing anodic tantalum oxide. Habazaki et al. [31] reported that the fluoride ions migrated inward at twice the rate of oxygen ions in growing anodic titanium oxide. As a consequence of the rapid inward migration of fluoride ions [32], the fluoride ions accumulate at the interface between the anodic oxide and Zr substrate to develop a fluoride-rich compact layer (1 h) [24, 33]. However, the content of F^- in electrolyte is decreasing during the anodization process, while OH^- and O^{2-}

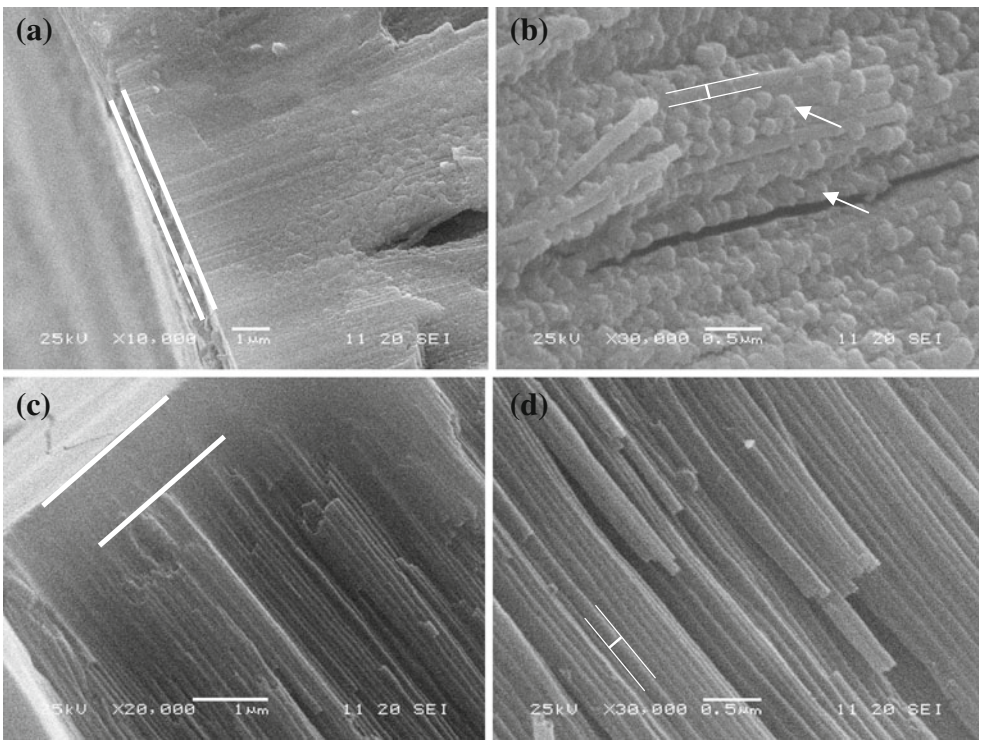

Fig. 5 SEM images of ZrO_2 nanotube arrays obtained by anodizing Zr foil in a mixture of glycerol and formamide (weight ratio=1:1) under 50 V for 1 h at **a**, **b** 0 °C and **c**, **d** 30 °C

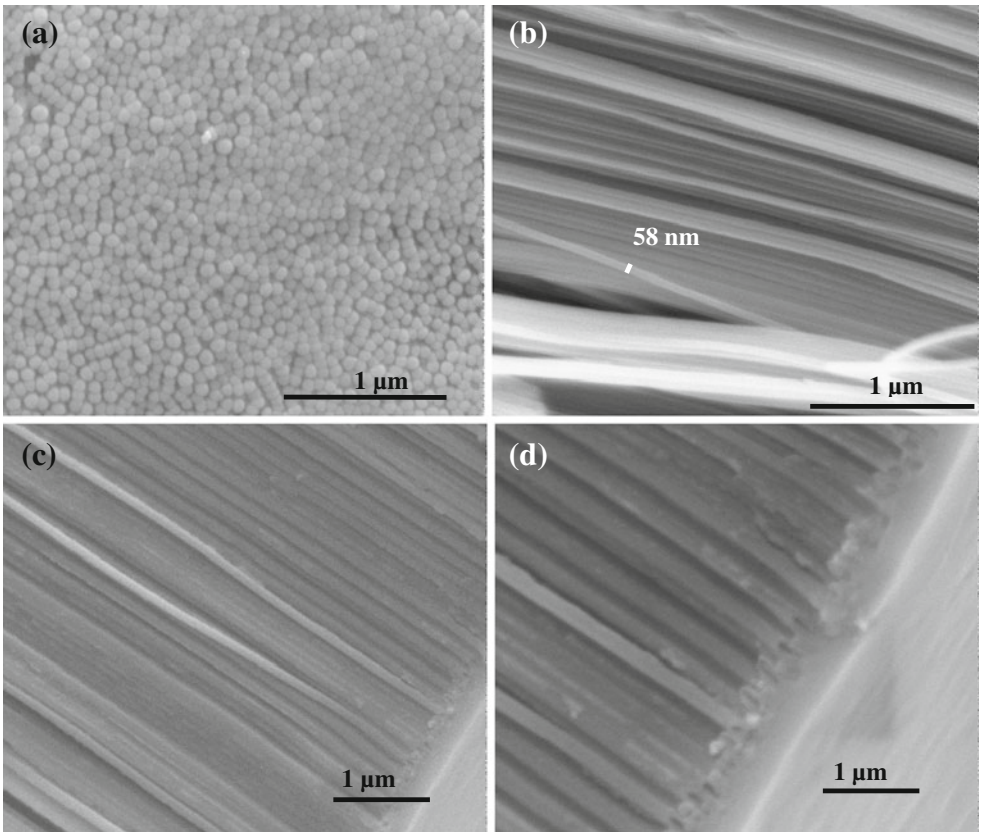

Fig. 6 SEM images of ZrO_2 nanotube arrays obtained by anodizing Zr foil fabricated in a mixture of glycerol and formamide (weight ratio=1:1) at room temperature in a mixture of formamide and glycerol (weight ratio=1:1) at **a**, **b** 20 V and **c**, **d** 60 V

gradually become more capable to compete with F^- to migrate inward, and thus the fluoride-rich compact layer disappears (3 h). For long anodization, the content of F^- in electrolyte is eventually not high enough to immediately dissolve the entire barrier layer at the electrolyte/ZrO_2 nanotube interface, and thus a random layer with many defects is formed (18 and 24 h). Meanwhile, the upper uniform tubular layer is dissolved during anodization, (ZrO_2+6 F^-+4H^+→ZrF_6^{2-}+2H_2O). Finally, the top uniform tubular layer completely disappears after 24 h of anodization.

In order to further investigate the formation mechanism of anodization, ZrO_2 nanotubes were fabricated in a mixture of glycol and formamide (weight ratio=4:1) at 50 V for 3 h. The morphology of ZrO_2 nanotubes is shown in Fig. 8a–e. From the cross-sectional view in Fig. 8b, c, it was observed that the O-ring-like extra parts are attached on the outer surface of the nanotubes, with a compact layer of 272-nm thickness under the tubular layer. Elemental EDX mapping in the scanning electron microscope [34] was further used to test the elemental distribution in the compact layer and the tubular layer. The distribution of oxygen is not homogeneous as more oxygen exists in the tubular layer than the compact layer, as shown in Fig. 8f. Inversely, more fluorine exists in the compact layer than the tubular layer, as shown in Fig. 8g. Therefore, the tubular layer is fabricated on the fluoride-rich compact layer in high electro-field to assist dissolution during anodization.

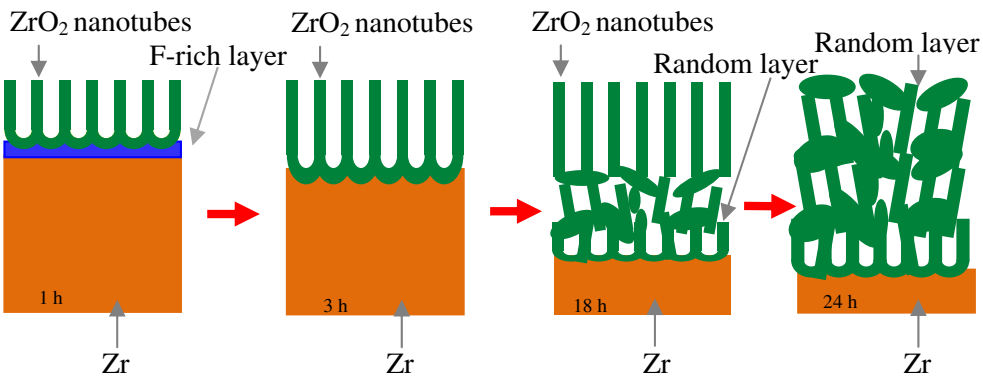

Fig. 7 A model representing the evolutions of morphology of ZrO_2 nanotube arrays on Zr substrate during anodization in a mixture of formamide and glycerol (weight ratio=1:1)

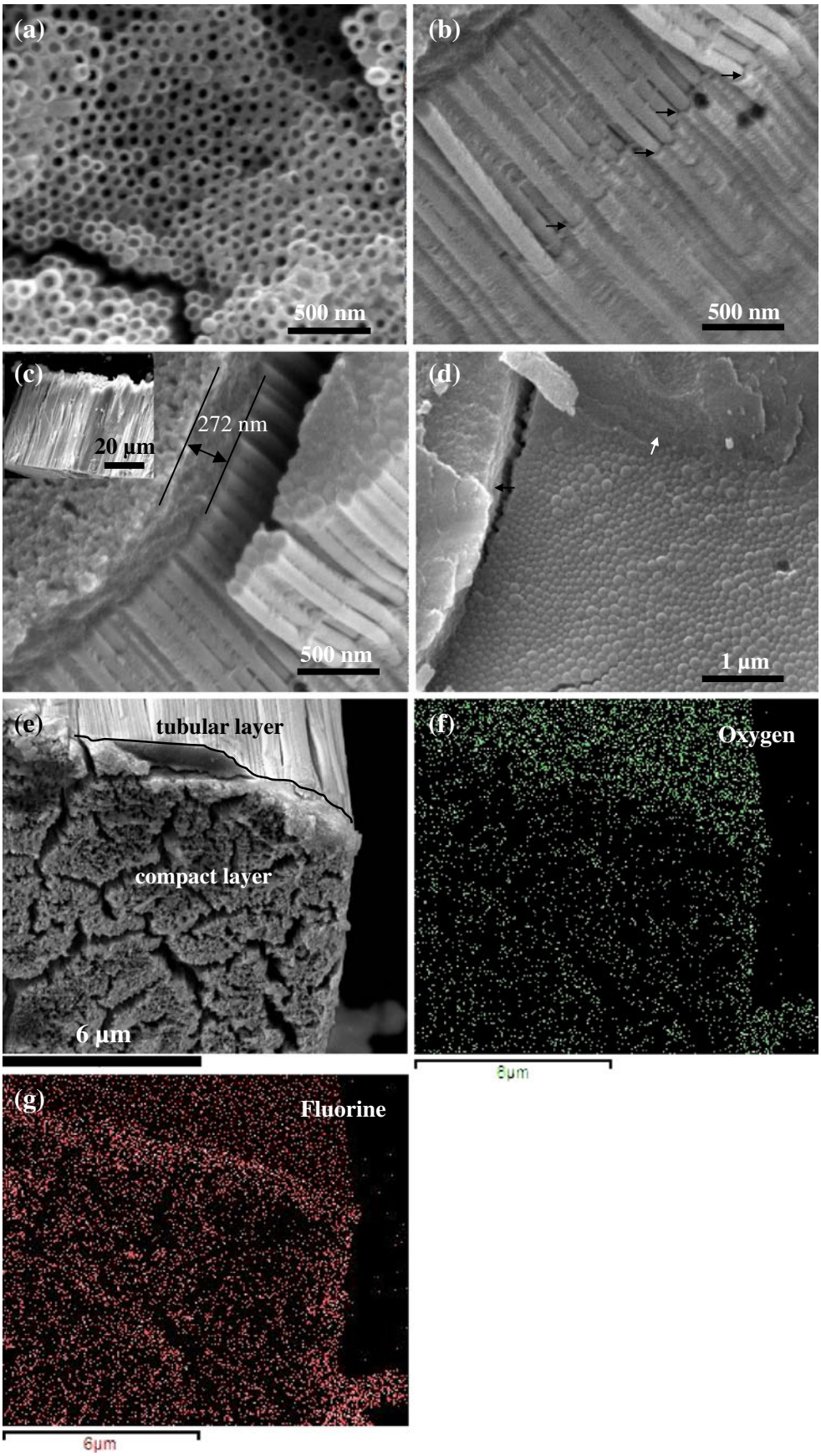

Fig. 8 SEM images of the top view (**a**), cross-sectional view (**b**, **c**), and bottom view (**d**, **e**) of ZrO_2 nanotubes fabricated in a mixture of glycol and formamide (weight ratio=4:1) under 50 V at room temperature for 3 h and then washed by D.I. water. The *inset* in **c** shows the thickness of the nanotubes. EDX element maps of oxygen (**f**) and fluorine (**g**) of the bottoms are shown in **e**

While as the compact layer cannot be completely dissolved during anodization, the retained compact layer yields O-rings on the outer surface of the nanotubes, and thus double-walled ZrO_2 nanotubes are formed.

The chemical compositions of the ZrO_2 compact layer formed in glycol and formamide (weight ratio=4:1) at 50 V for 3 h are characterized using XPS. The C 1 s peak at 284.6 eV is used as a reference binding energy for calibration. The ZrO_2 nanotube membrane is detached from the Zr substrate using an adhesion tape, and then the compact layer is on the top to test the XPS. The wide-survey scan X-ray photoelectron spectrum is shown in Fig. 9a. A series of peaks from Zr 4 s, Zr 3 d, Zr 3p, Zr 3 s, C 1 s, F 1 s, and O 1 s is clearly observed. Figure 9b–d is the high-resolution spectra of Zr 3 d, C 1 s, and F 1 s peaks, respectively. The Zr 3 d spectrum is broad and consists of two doublets. The lower binding energy doublet (at about 183.3 and 185.7 eV) corresponds to ZrO_2 species [35–37], while the higher binding energy doublet (around 184.8 and 187.2 eV) corresponds to Zr^{4+} linked to fluorine (ZrF_4) [38]. Zr metal (binding energy 178.6–179.6 eV) [39, 40] and ZrC (binding energy 178–179 eV) [40, 41] were not observed. The C 1 s region for ZrO_2 nanotubes is shown in Fig. 9c without evidence attributes to ZrC in the C 1 s region (C 1 s, 282 eV) [42], which indicates that C is a contamination induced from the nonaqueous electrolyte or during storage of the sample in air [43]. On the other hand, the F 1 s peak at 685.5 eV, as shown in Fig. 9d, is attributable to ZrF_4 [44, 45]. Recently, Muratore et al. [46, 47] fabricated anodic films on zirconium in 0.35 M NH_4F in glycerol and found that the ZrO_2 nanotubes were embedded in the fluoride-rich intratubular material. Therefore, the outer layer of the double-walled ZrO_2 nanotubes is probably the fluoride-rich layer.

Conclusion

In conclusion, uniform ZrO_2 nanotubes are successfully fabricated by 3 h of anodization in a mixture of glycerol and formamide (weight ratio=1:1) containing 1 wt.% NH_4F and 3 wt.% H_2O. The rate of fabricating ZrO_2 nanotubes decreases with the anodization time. A model to elucidate the morphological architecture evolution of ZrO_2 nanotubes on a Zr substrate during the anodization is presented. A thin fluoride-rich compact layer exists between the anodic zirconia oxide and the Zr substrate for 1 h of anodization. During the anodization process, the content of fluoride ions in electrolyte decreases, which may not be enough to immediately dissolve the entire barrier layer at electrolyte/oxide layer interface, and thus a random layer with many defects is formed instead of the uniform tubular layer. Since the fluoride-rich compact layer cannot be completely dissolved, the retained compact layer yields O-rings on the outer surface of the nanotubes with double walls.

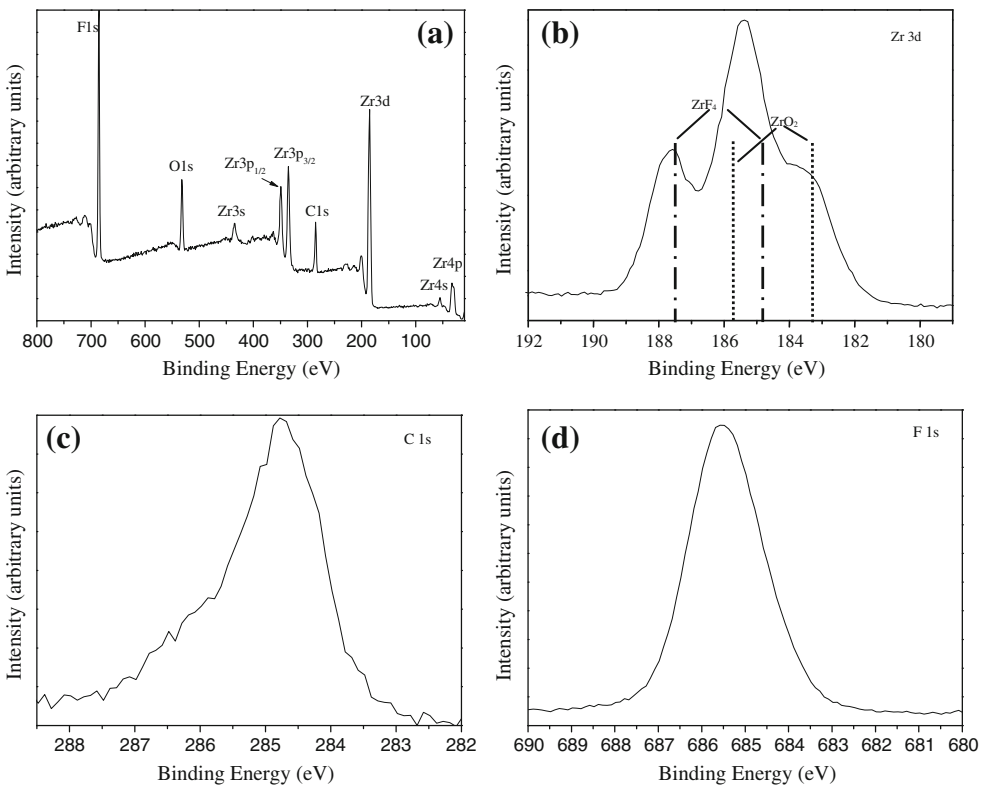

Fig. 9 A survey of XPS spectra of anodic ZrO_2 nanotubular arrays obtained in a mixture of glycol and formamide (weight ratio=4:1) under 50 V at room temperature (**a**), high-resolution spectra of Zr 3 d (**b**), C 1 s (**c**), and F 1 s (**d**)

Acknowledgements This work was supported by National Natural Science Foundation of China (No. 50772133), Innovation Projects for Graduates of Center South University (No. LA09014), and Scholarship Award for Excellent Doctoral Student granted by Ministry of Education of China (No. 1343–7113400102).

References

1. Weber J, Singhal R, Zekri S, Kumar A (2008) Intern Mater Rev 53:235–255
2. Fang D, Huang KL, Liu SQ, Qin DY (2009) Electrochem Commun 11:901–904
3. Allam NK, Feng XJ, Grimes CA (2008) Chem Mater 20:6477–6481
4. Karlinsey RL (2005) Electrochem Commun 7:1190–1194
5. Tsuchiya H, Macak JM, Sieber I, Schmuki P (2005) Small 1:722–725
6. Mukherjee N, Paulose M, Varghese OK, Mor GK, Grimes CA (2003) J Mater Res 18:2296–2299
7. Ghicov A, Schmuki P (2009) Chem Commun 20:2791–2808
8. Berger S, Jakubka F, Schmuki P (2009) Electrochem Solid State Lett 12:K45–K48
9. Bao J, Tie C, Xu Z, Ma Q, Hong J, Sang H, Sheng D (2002) Adv Mater 14:44–47
10. Shin HJ, Jeong DK, Lee JG, Sung MM, Kim JY (2004) Adv Mater 16:1197–1200
11. Cao W, Tan OK, Zhu W, Jiang B, Gopal RCV (2001) Sensor Actuat B Chem 77:421–426
12. Cho HJ, Choi GM (2008) J Power Sources 176:96–101
13. Tsai PC, Lee JH, Chang CL (2007) Surf Coat Technol 202:719–724
14. Fogaing EY, Huger M, Gault C (2007) J Eur Ceram Soc 27:1843–1848
15. Jin G, Lu G, Guo Y, Guo Y, Wang J, Kong W, Liu X (2005) J Mol Catal A: Chem 232:165–172
16. Tsuchiya H, Schmuki P (2004) Electrochem Commun 6:1131–1134
17. Fang D, Huang KL, Luo ZP, Wang Y, Liu SQ, Zhang QG (2011) J Mater Chem 21:4989–4994
18. Zhao JL, Wang XX, Xu RQ, Meng FB, Guo LM, Li YX (2008) Mater Lett 62:4428–4430
19. Shin Y, Lee S (2009) Nanotechnology 20:105301–105305
20. Guo L, Zhao J, Wang X, Xu R, Li Y (2009) J Solid State Electrochem 13:1321–1326
21. Tsuchiya H, Macak JM, Taveira L, Schmuki P (2005) Chem Phys Lett 410:188–191
22. Tsuchiya H, Macak JM, Ghicov A, Taveira L, Schmuki P (2005) Corros Sci 47:3324–3335
23. Vacandio F, Eyraud M, Chassigneux C, Knauth P, Djenizian T (2010) J Electrochem Soc 157:K279–K283
24. Muratore F, Wiecheć AB, Hashimoto T, Skeldon P, Thompson GE (2010) Electrochem Commun 12:1727–1730
25. Lockman Z, Sreekantan S, Ismail S, Schmidt-Mende L, MacManus-Driscoll JL (2010) J Alloy Compd 503:359–364
26. Pouporte T, Finne J (2006) J App Electrochem 36:33–41
27. Khalil N, Leach JS (1996) J App Electrochem 26:231–233
28. Ismail S, Ahmad ZA, Berenov A, Lockman Z (2011) Corr Sci 53:1156–1164
29. O'Sullivan JP, Wood GC (1970) Proc Roy Soc Lond A 317:511–543
30. Shimizu K, Kobayashi K, Thompson GE, Skeldon P, Wood GC (1997) J Electrochem Soc 144:418–423
31. Habazaki H, Fushimi K, Shimizu K, Skeldon P, Thompson GE (2007) Electrochem Commun 9:1222–1227
32. Albu SP, Ghicov A, Aldabergenova S, Drechsel P, LeClere D, Thompson GE, Macak JM, Schmuki P (2008) Adv Mater 20:4135–4139
33. Berger S, Kunze J, Schmuki P, Valota AT, LeClere DJ, Skeldon P, Thompson GE (2010) J Electrochem Soc 157:C18–C23
34. Mahesh RA, Jayaganthan R, Prakash S (2009) J Alloys Comp 468:392–405
35. Stefanov P, Stoychev D, Valov I, Kakanakova-Georgieva A, Marinova T (2000) Mater Chem Phys 65:222–225
36. Suzuki S, Yanagihara K, Hirokawa K (2000) Surf Interface Anal 30:372–376
37. Cho BO, Lao S, Sha L, Chang JP (2001) J Vac Sci Technol A 19:2751–2761
38. Ardelean H, Frateur I, Zanna S, Atrens A, Marcus P (2009) Corr Sci 51:3030–3038
39. Ebert H, Knecht M, Muhler M, Helmer O, Bensch W (1995) J Phys Chem 99:3326–3330
40. Steiner SA, Baumann TF, Bayer BC, Blume R, Worsley MA, MoberlyChan WJ, Shaw EL, Schlogl R, Hart AJ, Hofmann S, Wardle BL (2009) J Am Chem Soc 131:12144–12154
41. Balaceanu M, Braic M, Braic V, Vladescu A, Negrilaa CC (2005) J Optoelectron Adv Mater 7:2557–2560
42. Won YS, Kim YS, Varanasi VG, Kryliouk O, Anderson TJ, Sirimanne CT, McElwee-White L (2007) J Cryst Growth 304:324–332
43. Li LJ, Yan DX, Lei JL, He JX, Wu SM, Pan FS (2011) Mater Lett 65:1434–1437
44. Cong P, Mori S (2004) Tribol Lett 17:261–267
45. Wang LN, Luo JL (2010) Electrochem Commun 12:1559–1562
46. Muratore F, Hashimoto T, Skeldon P, Thompson GE (2011) Corr Sci 53:2299–2305
47. Muratore F, Baron-Wiechec A, Hashimoto T, Gholinia A, Skeldon P, Thompson GE (2011) Growth of nanotubes on zirconium in glycerol/fluoride electrolytes. Electrochim Acta. doi:10.1016/j.electacta.2010.12.089